# Soil moisture-atmosphere feedbacks mitigate projected surface water availability declines in drylands

Sha Zhou[1,2,3,4,5*], A. Park Williams[1], Benjamin R. Lintner[6], Alexis M. Berg[7], Yao Zhang[4,5], Trevor F. Keenan[4,5], Benjamin I. Cook[1,8], Stefan Hagemann[9], Sonia I. Seneviratne[10], Pierre Gentine[2,3]

[1]Lamont-Doherty Earth Observatory of Columbia University, Palisades, NY, USA

[2]Earth Institute, Columbia University, New York, NY, USA

[3]Department of Earth and Environmental Engineering, Columbia University, New York, NY, USA

[4]Climate and Ecosystem Sciences Division, Lawrence Berkeley National Laboratory, Berkeley, CA, USA

[5]Department of Environmental Science, Policy and Management, UC Berkeley, Berkeley, CA, USA

[6]Department of Environmental Sciences, Rutgers, The State University of New Jersey, New Brunswick, NJ, USA

[7]Department of Earth and Planetary Sciences, Harvard University, Cambridge, MA, USA

[8]NASA Goddard Institute for Space Studies, New York, NY, USA

[9]Helmholtz-Zentrum Geesthacht, Institute of Coastal Research, Geesthacht, Germany

[10]Institute for Atmospheric and Climate Science, ETH Zurich, Zurich, Switzerland

*Correspondence to: sz2766@columbia.edu

**Global warming alters surface water availability (precipitation minus evapotranspiration, P-E) and hence freshwater resources. However, the influence of land-atmosphere feedbacks**

**on future P-E changes and the underlying mechanisms remain unclear. Here we demonstrate that soil moisture (SM) strongly impacts future P-E changes, especially in drylands, by regulating evapotranspiration and atmospheric moisture inflow. Using modeling and empirical approaches, we find a consistent negative SM feedback on P-E, which may offset ~60% of the decline in dryland P-E otherwise expected in the absence of SM feedbacks. The negative feedback is not caused by atmospheric thermodynamic responses to declining SM, but rather reduced SM, in addition to limiting evapotranspiration, regulates atmospheric circulation and vertical ascent to enhance moisture transport into drylands. This SM effect is a large source of uncertainty in projected dryland P-E changes, underscoring the need to better constrain future SM changes and improve representation of SM-atmosphere processes in models.**

Future changes in water availability pose great challenges to global freshwater and food security and the sustainability of natural ecosystems[1,2]. Changes in precipitation and evapotranspiration are especially important for dryland ecosystems where vegetation growth and mortality largely depend on water availability[3,4]. Global warming is expected to intensify the global water cycle[5–7], but the projected changes in surface water availability, namely precipitation minus evapotranspiration (P-E), exhibit divergent spatial patterns between ocean and land[8,9]. Over the ocean, projected P-E changes broadly follow the "dry-get-drier, and wet-get-wetter" (DDWW) paradigm, driven by increasing atmospheric moisture content and transport by the mean circulation in a warming climate[5,6]. However, thermodynamic mechanisms cannot effectively explain P-E changes over land, where the magnitudes of the P-E response to warming are much smaller than over the ocean[8,9]. Circulation anomalies driven by sea surface temperature changes have been demonstrated to cause

deviations from the "wet-get-wetter" response in the wet tropics[10–12], but the dynamic mechanisms of dryland P-E changes, and their potential dependence on land surface feedbacks, are not well understood.

In water-limited regions, soil moisture (SM) directly regulates evapotranspiration, which may positively feed back onto precipitation via moisture recycling[13,14]. SM may also impact precipitation through its influence on boundary layer dynamics and mesoscale circulations[15–18]. For example, spatial gradients in SM and associated sensible heat flux gradients may preferentially promote convection over drier soils relative to surrounding wetter soils, resulting in a negative SM feedback on precipitation[15,18,19]. However, the sign of the SM-precipitation feedback can change in the presence of a background wind that enables the propagation of convective cells to neighboring regions[20]. Given that various processes may lead to short-term SM-precipitation feedbacks of opposing sign and/or varying strength, it is challenging to extrapolate the effects of these processes to longer timescales. The long-term (climatological) SM effects on P-E have yet to be diagnosed, particularly under future global warming.

Here we directly assess the long-term SM effect on future model-projected P-E using four general circulation models included in the Global Land Atmosphere Coupling Experiment (GLACE)-CMIP5[21] as well as simulations from 35 general circulation models in CMIP5 (Methods and Table S1). We quantify the SM contribution to P-E changes between 30-year historical (1971-2000) and future (2071-2100, RCP8.5) periods using three sets of model experiments in GLACE-CMIP5: a reference simulation (REF) with SM fully interactive with the atmosphere, and two perturbation simulations where the SM climatology is prescribed as the 1971-2000 climatology (expA) and a

centered, 30-year running mean climatology from REF (expB) (Fig. S1). For each of the four models, the three simulations are driven by the same forcing agents (i.e., sea surface temperatures, sea ice, land use, and $CO_2$ concentrations), allowing us to compare them to isolate the total SM effect (REF-expA) and the effects of SM trends (expB-expA) and variability (REF-expB) on P-E changes. We further develop a multiple linear regression model to assess the sign and strength of the SM-(P-E) feedback and identify the primary feedback pathways by comparing SM effects on atmospheric dynamic and thermodynamic processes using two observationally constrained reanalysis products (MERRA-2 and ERA5) that provide pressure level, wind and humidity data in recent decades (1979-2018). These pressure level data are not available in GLACE-CMIP5.

**Soil moisture effect on future P-E changes in model projections**

The 35 CMIP5 models show significant ($p<0.05$, Student's t-test) P-E increases in 42% of wet regions and P-E declines in 51% of dry regions over ocean between the historical and future periods (Fig. 1a and Fig. S2e). Over land, future P-E is projected to increase significantly ($p<0.05$) in high-latitude wet regions, but its change is insignificant over 93% of dry regions. Here "dry" versus "wet" regions are characterized as negative versus positive P-E over ocean, and drylands versus non-drylands over land (Methods and Fig. S2a-d). Unlike P-E changes, significant ($p<0.05$) SM changes are projected over 33% of drylands (Fig. 1b). Such SM changes directly impact evapotranspiration and may potentially feed back onto precipitation, both of which are expected to play a role in the projected P-E changes over land.

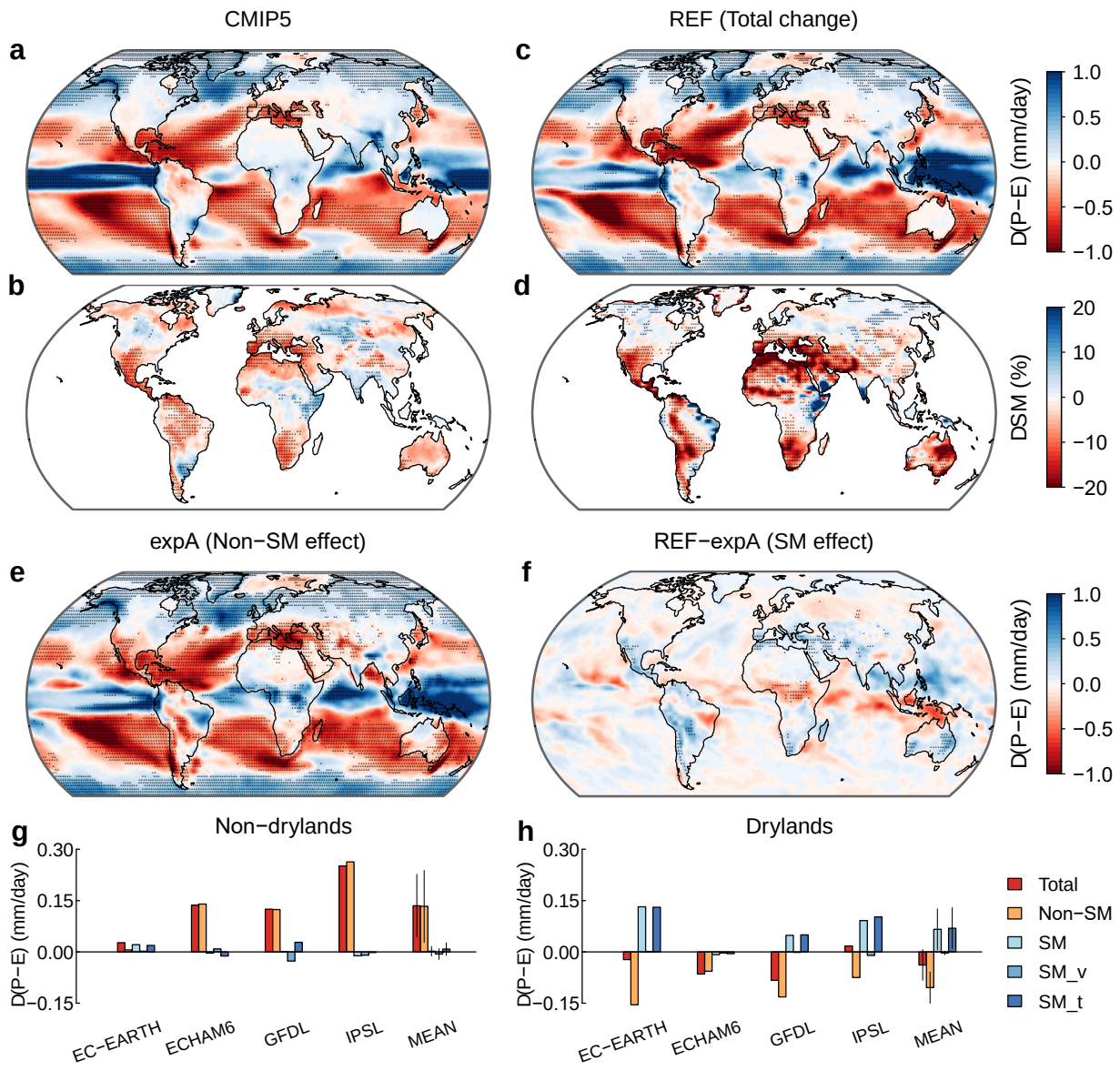


91

92 **Figure 1. Multi-model mean annual changes in surface water availability and soil moisture.**

93 **a**-**b**, Changes in precipitation minus evapotranspiration (Δ(P-E), a) and percent changes in total

94 soil moisture (ΔSM, b) between historical (1971-2000) and future (2071-2100, RCP8.5) periods

95 (future minus historical values) in 35 CMIP5 models. **c**-**f**, The same as **a**-**b**, but for REF of the four

96 GLACE-CMIP5 models (**c**-**d**), and Δ(P-E) induced by non-SM factors (expA, **e**) and SM (REF-

97 expA, **f**). **g**-**h**, Total area-weighted Δ(P-E) and the contributions from non-SM factors, total SM

98 changes, SM variability (SM_v) and SM trends (SM_t) across non-drylands (**g**) and drylands (**h**)

in the four GLACE-CMIP5 models. The error bar shows the standard deviation of Δ(P-E) across the four models. Stippling denotes regions where the change in P-E is significant at the 95% level (Student's t-test) and the sign of the change is consistent with the sign of multi-model means (as shown in the figure) in at least 21 of the 35 (60%) CMIP5 models (**a**-**b**), and at least three of the four GLACE-CMIP5 models (**c**-**f**).

The spatial patterns of P-E and SM changes in REF of the four GLACE-CMIP5 models are largely consistent with the broader suite of CMIP5 models (Fig. 1a-d and Fig. S2e,f), with spatial correlation coefficients of 0.82 for P-E over all grid cells and 0.35 for SM. In expA, in which the mean annual cycle of SM over the historical period is imposed throughout the entire simulation, the DDWW paradigm holds over 31% of the land regions, compared to only 19% of land areas showing DDWW in REF (Fig. 1c,e and Fig. S2f,g). In particular, the proportion of drylands showing significant P-E declines in expA (30%) is three times that in REF (10%). Since P-E changes in expA are driven by factors excluding SM trends and variability, such as temperature-driven oceanic and atmospheric changes, we denote these factors collectively as non-SM effects.

On the other hand, we isolate the SM effect on projected P-E changes by differencing the REF and expA simulations. The SM effects on projected P-E changes generally oppose the non-SM effects in expA (Fig. 1e,f), with spatial correlation coefficients ranging from -0.40 to -0.69 across the four models. The future SM changes and the P-E changes induced by SM are of opposite sign for multi-model means (Fig. 1d,f), and for each model (Fig. S3) and season (Fig. S4), indicating a negative SM feedback on P-E. P-E changes induced by non-SM factors are partially cancelled by the negative SM feedback on P-E, especially in drylands, where the SM-induced P-E increases in REF

(0.066±0.060 mm/day, mean±1s.d.) offset 63% of the P-E declines (-0.104±0.046 mm/day) that would be otherwise induced by the non-SM factors simulated in expA (Fig. 1h). This offset effect is dominated by the negative SM trends over drylands (Fig. 1d), with minimal effect from changes in higher-frequency SM variability (Fig. 1h). The mitigating effect of declining SM on dryland P-E reduction is large in EC-EARTH (85%), GFDL (37%) and IPSL (123%), but no such effect is found in ECHAM6 because that model projects increased SM that reduces P-E in many tropical drylands (Fig. S3b,f,j). Outside of drylands, P-E changes are generally dominated by non-SM factors (Fig. 1g).

Comparing the SM effects on precipitation and evapotranspiration, the decline in evapotranspiration (-0.163±0.083 mm/day) induced by future SM drying is roughly twice as large as the SM drying effect on precipitation (-0.097±0.052 mm/day) over drylands (Fig. S5). This stronger SM limitation on evapotranspiration than on precipitation indicates that the positive feedback of SM on precipitation via moisture recycling—or lower precipitation with future SM decline—is partially offset by other atmospheric responses to SM, as we discuss further in the following section.

**Mechanisms of the soil moisture impact on P-E changes**

Multiple theories have been postulated to explain future P-E changes over land, many of which focus on thermodynamic mechanisms, including warming-driven changes in specific humidity and land-ocean warming contrast[22–24]. Circulation changes, such as shifts in the strength of Walker and Hadley circulations, are also invoked to explain deviations of P-E changes from expected thermodynamic responses over land[10–12,25–28], but these dynamic mechanisms are predominantly

driven by sea surface warming. Our finding of a strong SM effect on future P-E changes is not readily explained by these mechanisms. A recent study proposed an extended thermodynamic scaling of P-E changes including both local specific humidity changes and the horizontal gradient of specific humidity, but this extended scaling tends to overestimate both P-E decreases in drylands and P-E increases in the wet tropics[9], similar to the projected P-E changes by ocean-atmosphere processes in expA (Fig. 1e). This indicates that the thermodynamic effect does not fully capture the SM effect on P-E changes; rather, dynamic effects related to SM are necessary to account for these changes.

To test this hypothesis, we explore the thermodynamic and dynamic mechanisms of P-E changes driven by long-term SM trends in GLACE-CMIP5. Relative to expA, which lacks long-term SM trends, expB manifests greater temperature increases but weaker specific humidity increases (Fig. 2a-d). The SM effect is especially strong over drylands where negative trends in SM lead to reduced evapotranspiration and evaporative cooling (Fig. S5b), which are consistent with the enhanced warming and reduced moistening in expB compared to expA (Fig. 2a-d). An SM-induced horizontal gradient of specific humidity is expected to induce more moisture into drylands by landward moisture flux, according to the extended thermodynamic scaling of P-E changes[9]. However, this negative effect may be partially or totally offset by local specific humidity reductions.

We examine the SM impact on atmospheric dynamic processes by comparing future changes in the vertical profile of vertical motion (here quantified in terms of $-\omega$, the negative pressure velocity) over drylands between expA and expB in the IPSL model. Both simulations project enhanced

ascent throughout the lower troposphere over drylands in the future, which is of greater magnitude in expB compared to expA (Fig. 2e). In particular, the SM effect on future P-E changes is largely consistent with that on tropospheric vertical ascent, with spatial correlation coefficients ranging from 0.37 to 0.59 over drylands (Fig. S6). In each season, the spatial pattern of the SM effect on vertical ascent is also positively correlated with that on future P-E changes over drylands, especially in summer (wet season) (Fig. S7). Although the SM effects on vertical ascent and P-E vary seasonally/geographically and across models, the IPSL results support the notion that reduced SM may promote atmospheric vertical ascent, potentially contributing to the negative SM effect on P-E.

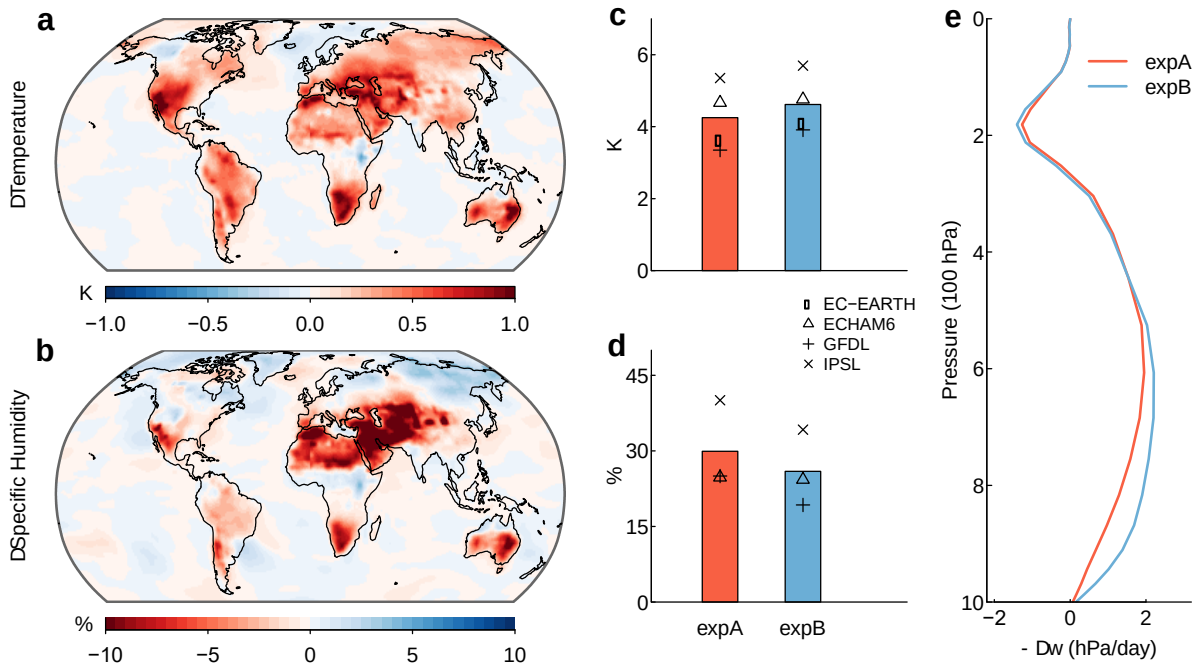


**Figure 2. Soil moisture effects on changes in temperature, specific humidity, and vertical ascent in GLACE-CMIP5. a**,**b**, Multi-model mean soil moisture effects (expB-expA) on projected changes (Δ) in temperature and specific humidity from historical (1971-2000) to future (2071-2100) periods (future minus historical values). **c**,**d**, Projected changes in temperature and specific humidity over drylands in expA and expB (bars: multi-model mean, symbols: individual

183 models, specific humidity is not available in EC-EARTH). Changes to specific humidity are
184 expressed fractionally relative to their historic period values (in percentages). **e**, Projected changes
185 in negative pressure velocity ($-\Delta\omega$) over drylands in expA and expB for the IPSL model.
186
187 **Thermodynamic versus dynamic effects in the soil moisture-(P-E) feedback**
188 To further compare the thermodynamic and dynamic mechanisms of the negative SM-(P-E)
189 feedback, we analyze the SM impact on the atmospheric moisture budget from the observationally
190 constrained MERRA-2 and ERA5 reanalysis products. We apply a statistical framework to identify
191 the SM feedback on P-E at the monthly scale, and to isolate the SM effects on the thermodynamic
192 and dynamic components of P-E variations. We establish a multiple linear regression model to
193 determine the sign and strength of the SM-(P-E) feedback, which is represented by a sensitivity
194 coefficient that measures the partial derivative of standardized P-E variations to standardized SM
195 variations in the previous month (Methods). A sensitivity coefficient of 0.1 indicates that P-E
196 increases by 10% of its standard deviation when previous-month SM increases by one standard
197 deviation.
198
199 Consistent with the experimental results in Fig. 1, we find widespread negative sensitivity
200 coefficients for SM$\rightarrow$(P-E), i.e., the effect of SM on P-E, in the fully coupled simulations of
201 GLACE-CMIP5 models and reanalysis products, with significant effects in the subtropical and
202 mid-latitude dry regions (Fig. 3a,d,g). We further compare SM$\rightarrow$E and SM$\rightarrow$P. As expected, SM
203 exerts a strong positive impact on evapotranspiration, while its effect on precipitation is much
204 weaker (Fig. 3b,c,e,f,h,i), because precipitation is strongly controlled by large-scale atmospheric
205 dynamics. Besides evapotranspiration, atmospheric moisture convergence (MC) is the other source

of moisture for precipitation. We find consistent negative SM→MC in MERRA-2 and ERA5 (Fig. 3j,m). As monthly SM variations strongly and positively force evapotranspiration but generally negatively affect moisture convergence, SM has a more muted effect on precipitation than on evapotranspiration, resulting in a negative SM-(P-E) feedback.

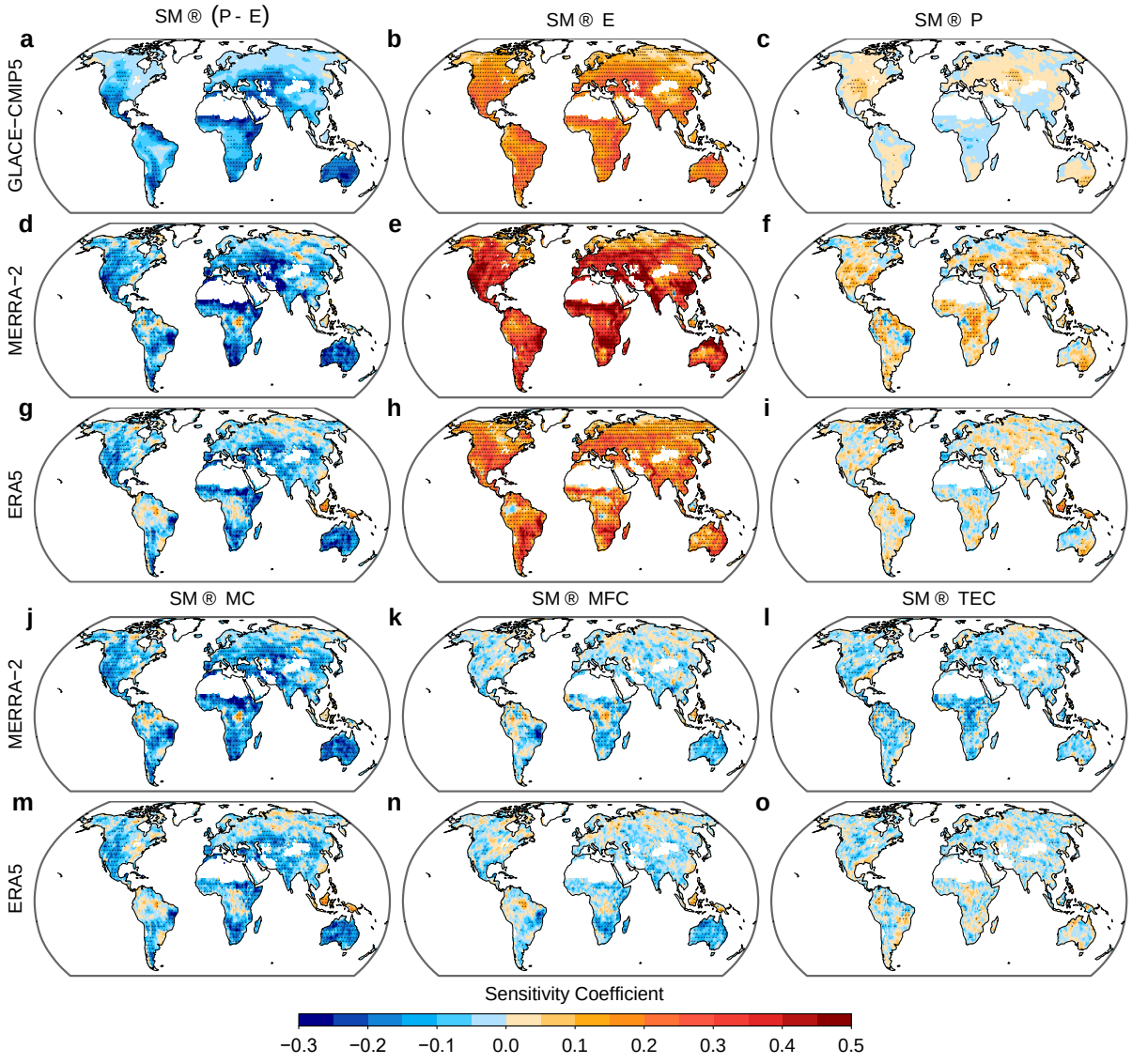


**Figure 3. Soil moisture feedbacks on water availability in GLACE-CMIP5 models and reanalysis datasets. a-f**, Sensitivity coefficients for soil moisture (SM)→precipitation minus evapotranspiration (P-E), SM→evapotranspiration (E) and SM→precipitation (P) identified based

on REF of the four GLACE-CMIP5 models (1971-2100) (**a-c**), MERRA-2 (1980-2018) (**d-f**) and ERA5 (1979-2018) (**g-i**). Mean values of the sensitivity coefficients produced by the four models are shown in **a-c**. **j-o**, the same as **d-i**, but for SM→moisture convergence (MC) (**j**,**m**), SM→mean flow convergence (MFC) (**k**,**n**), and SM→transient eddy convergence (TEC) (**l**,**o**). The sensitivity coefficient for X→Y denotes the partial derivative of standardized Y to standardized X in the previous month, where the seasonal cycles and long-term trends in X and Y are removed. Stippling denotes regions where the sensitivity coefficient is significant at the 95% level according to a bootstrap test. In **a-c**, stippling denotes regions where the sensitivity coefficient is significant at the 95% level and the sign of the sensitivity coefficient is consistent with the sign of multi-model means (as shown in the figure) in at least three of the four GLACE-CMIP5 models.

Although atmospheric moisture storage changes on monthly scales, the change is relatively small; thus monthly P-E approximately balances moisture convergence. The latter is calculated as the negative divergence ($\nabla$) of vertically mass-integrated moisture flux from the top of the atmosphere ($p = 0$) to the surface ($p = p_s$), i.e.,

$$P - E \approx -\frac{1}{\rho_w g} \nabla \cdot \int_0^{p_s} (\overline{\boldsymbol{u}}\,\overline{q} + \overline{\boldsymbol{u}'q'}) dp \quad (1)$$

where $\rho_w$ is the density of water, $g$ is the acceleration due to gravity, $\boldsymbol{u}$ is the horizontal vector wind, and $q$ is specific humidity. Moisture convergence on the right side of equation (1) is decomposed into mean flow convergence determined by monthly mean wind ($\overline{\boldsymbol{u}}$) and moisture ($\overline{q}$) fields, and transient eddy convergence associated with highly variable wind ($\boldsymbol{u}'$) and moisture ($q'$) fields within storm systems[29,30]. We find negative SM effects on mean flow convergence and transient eddy convergence across 60-73% of the assessed land area, contributing to the negative

SM→MC over more than 75% of the land area (Fig. 3j-o). As moisture flux by transient eddies is approximately diffusive[31], a negative SM influence on the transient eddy convergence may be expected based on horizontal diffusion of water vapor along specific humidity gradient into a dry air column above dry soils, but could also arise from atmospheric circulation responses.

To understand how changing SM impacts mean flow convergence, we decompose monthly variations of this quantity into a thermodynamic component induced by moisture changes ($\overline{\boldsymbol{u}}\delta\bar{q}$), a mean circulation dynamic component induced by wind changes ($\bar{q}\delta\overline{\boldsymbol{u}}$), and a covariation component by the product of monthly mean moisture and wind changes ($\delta\overline{\boldsymbol{u}}\delta\bar{q}$)[30]. The negative SM feedback on mean flow convergence arises principally from the dynamic component (Fig. 4a,f): reduced SM enhances surface heating, thereby promoting vertical ascent and associated low-level flow convergence, particularly in dry regions (see SM→negative pressure velocity in Fig. 4d,i). The dynamic component is negative across most land regions. In contrast, the SM effect on the thermodynamic component largely depends on the mean flow environment. Increasing SM increases atmospheric humidity, thus inducing greater moisture convergence (divergence) by the thermodynamic effect when the mean low-level flow is convergent (divergent) (Fig. 4b,g,e,j). This explains why the thermodynamic component of mean flow convergence acts as a positive feedback in tropical convergence zones but as a negative feedback where the mean flow is divergent. The covariation component is weaker and more spatially variable (Fig. 4c,h). Moreover, using an attribution method based on variance decomposition (Methods), we find monthly moisture convergence variations are again dominated by the dynamic component, while the contributions from other components are relatively small (Fig. S8). These results indicate that the negative SM

effect on moisture convergence and P-E is mainly determined by the SM regulation of atmospheric circulation.

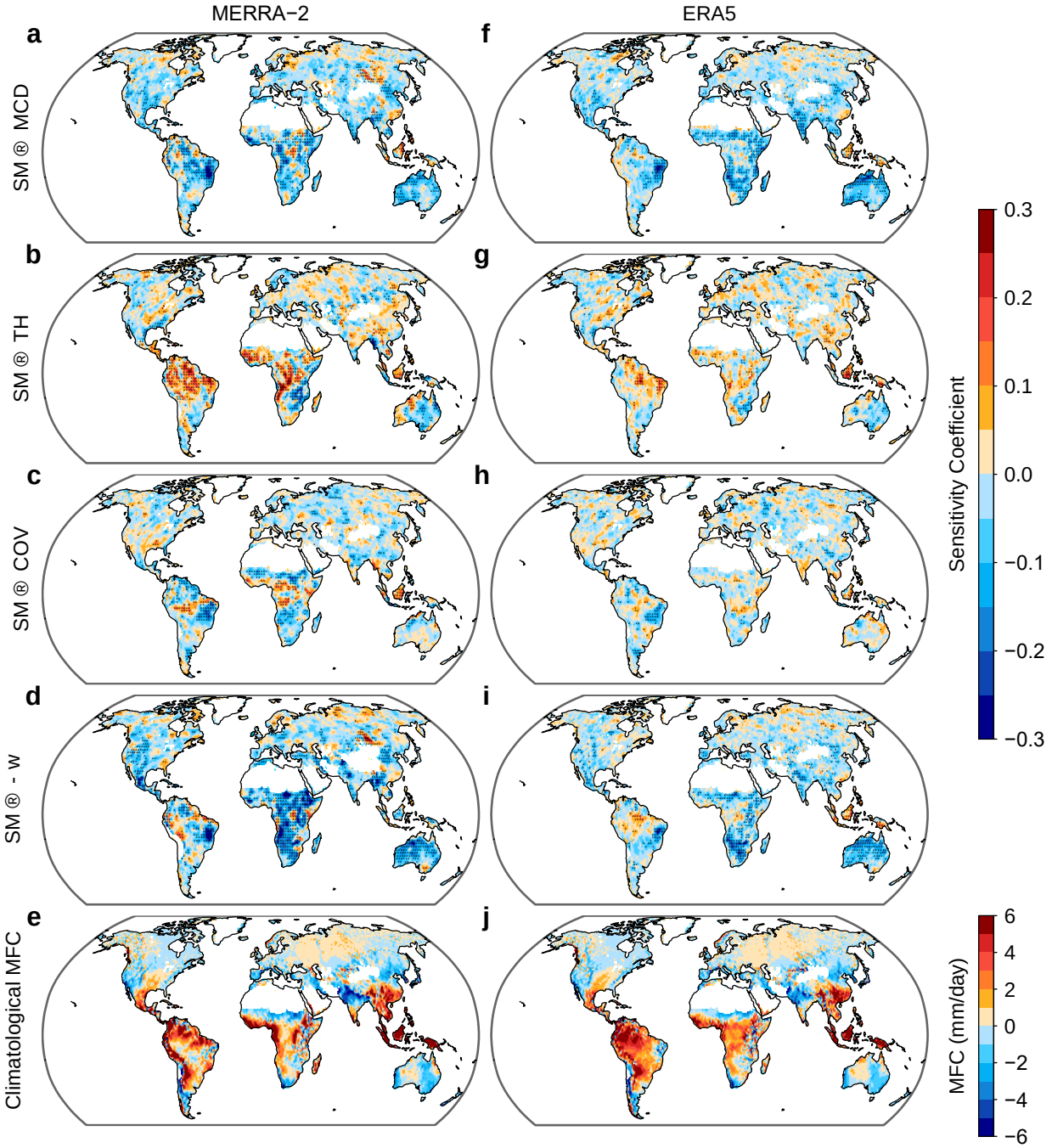


**Figure 4. Soil moisture effects on the three components of mean flow convergence. a-e**, Sensitivity coefficients for soil moisture (SM)→mean circulation dynamic component (MCD) (**a**),

SM→thermodynamic component (TH) (**b**), SM→covariation component (COV) (**c**), SM→negative pressure velocity (-ω) at 700 hPa (middle troposphere) (**d**), and climatological monthly mean flow convergence (MFC) (**e**) in MERRA-2 (1980-2018). **f-j**, the same as **a-e**, but for ERA5 (1979-2018). The sensitivity coefficient for X→Y denotes the partial derivative of standardized Y to standardized X in the previous month, where the seasonal cycles and long-term trends in X and Y are removed. Stippling in **a-d** and **f-i** denotes regions where the sensitivity coefficient is significant at the 95% level according to a bootstrap test.

## Discussion and implications

We demonstrate that long-term SM trends strongly influence future P-E changes, particularly over drylands. Projected reductions in dryland SM directly limit evapotranspiration and reduce moisture recycling for precipitation, but reduced SM also enhances moisture convergence, which partly counteracts precipitation declines driven by reduced evapotranspiration. These processes result in a weaker SM limitation on precipitation than on evapotranspiration, and a robust negative SM-(P-E) feedback at monthly and climatological scales. Without feedbacks from declining SM, future P-E changes would agree with the DDWW response to global warming over 31% of the land regions (Fig. 1 and Fig. S2). However, the negative SM feedback on P-E partially offsets declines in P-E via non-SM factors over drylands, while slightly attenuating P-E increases experienced over many non-drylands, resulting in only 19% of the land regions showing the DDWW pattern.

To interpret future P-E changes over land, recent studies have emphasized the importance of land-ocean warming contrast[9,22,24], which affects the spatial pattern of atmospheric moisture content and P-E responses, in addition to local warming-driven P-E changes. The projected decline in

dryland SM enhances the land-ocean warming contrast through enhanced land region warming, but thermodynamic mechanisms alone cannot well explain the negative SM feedback on P-E. Rather, we demonstrate that the negative SM-(P-E) feedback occurs mainly through SM induced changes in evapotranspiration as well as changes to the surface energy balance that modify the mean circulation, as declining SM enhances low-level vertical ascent and moisture convergence via associated low-level flow convergence. This dynamic effect may also be tied to declining SM reducing evapotranspiration and supporting a larger land-ocean warming contrast, which strengthens the landward pressure gradient and drives greater low-level moisture transport from the ocean to land[32–34].

The negative SM feedback on P-E has important implications for hydroclimatic variability[35]. From our analysis of GLACE-CMIP5 simulations, the magnitudes and frequencies of both extreme high and extreme low P-E are enhanced in the expA simulations relative to the REF (Fig. S9). The expA simulations only include non-SM effects of oceanic and atmospheric processes, while in REF, SM variations have a positive effect on evapotranspiration but a negative feedback on moisture convergence: thus, hydroclimatic variability is muted when SM feedbacks operate. Of course, while the negative SM feedback on P-E reduces the magnitudes and frequencies of extreme P-E events in drylands, extreme hydroclimatic events, such as droughts and floods, are still projected to increase in some regions in a warmer climate[36,37].

Our study highlights the importance of soil moisture changes and the associated soil moisture-atmosphere feedbacks in future projections of surface water availability. Although fully coupled general circulation models do include the negative soil moisture feedback on surface water

availability over drylands, the feedback strength, as well as the soil moisture projections themselves, are highly variable and model dependent (Fig. S3), leading to large uncertainty in how changes in soil moisture will affect future surface water availability (Fig. 1). In particular, we find that soil moisture variations contribute a larger proportion than other oceanic and atmospheric drivers (0.060 versus 0.046 mm/day, s.d. in Fig. 1h) to cross-model variations in the projected changes in dryland water availability. This points to the need for improved modelling of soil moisture trends and variability, which may be achieved through refined representation of land-atmosphere processes in general circulation models, especially the coupling between soil moisture, evapotranspiration, atmospheric circulation, and the hydrological cycle. Accurate model representation of soil moisture and the associated soil moisture-atmosphere feedbacks is crucial for providing reliable projections of surface water availability for better water resources management, and for mitigating future challenges of increasing water scarcity over drylands.

## Materials and Methods

**CMIP5 model simulations.** We used 35 CMIP5 models (listed in Table S1) covering the historical (1971-2000) and future (2071-2100, RCP8.5 high emissions scenario) periods. The ensemble member "r1i1pi" was used for each model. These models were selected because they provide the monthly total soil moisture content, precipitation, and latent heat flux required for our analyses. Evapotranspiration was calculated from latent heat flux in each model. We calculated multi-model mean annual changes in these variables between the historical and future periods.

**GLACE-CMIP5 experiments.** We used simulations from four models (i.e., EC-EARTH, ECHAM6, GFDL and IPSL) that participate in the GLACE-CMIP5 experiment, which was

performed to assess the impact of SM-climate feedbacks in CMIP5 projections[21] and has been widely used to isolate the SM effect on the atmosphere[38–40]. We did not use the other two models (ACCESS and CCSM4) in the GLACE-CMIP5 experiment because of problems with the prescribed SM. In each model, we used three simulations, i.e., a reference simulation (REF) and two perturbation simulations (expB and expA), covering the period from 1950 to 2100. All three simulations were driven by prescribed sea surface temperature, sea ice, land use, and $CO_2$ concentrations from the respective CMIP5 simulations (the historical simulations over 1950-2005 and the RCP8.5 scenario over 2006-2100). The difference between the three simulations is that SM was fully coupled with the atmosphere in REF, while SM climatology was prescribed as the 1971-2000 climatology (expA) and a centered, 30-year running mean climatology from REF (expB) in the two perturbation simulations (Fig. S1). Comparing simulated atmospheric variables between the three simulations, we could isolate the effects of SM trends (expB-expA) and variability (REF-expB) and total SM effect (REF-expA) due to SM-atmosphere feedbacks.

For our analyses, we used monthly total soil moisture content, precipitation, and latent heat flux from the three simulations in each model. Evapotranspiration was calculated from latent heat flux in each simulation. Multi-model mean annual changes in SM between the historical and future periods in REF were compared with those from CMIP5. In each model, we calculated mean annual changes in precipitation, evapotranspiration, and P-E between the historical and future periods in the three simulations. We isolated the contributions of total SM changes (REF-expA), SM trends (expB-expA), and SM variability (REF-expB) to future changes in these variables. To investigate the mechanisms behind the SM effect on P-E changes, we used near-surface (2m) temperature, specific humidity, and the vertical profile of pressure velocity from expA and expB. Temperature

355 is available in all four models, but specific humidity is not archived in EC-EARTH, and pressure
356 velocity is only available in IPSL.
357
358 **Reanalysis datasets.** To identify the SM feedback on P-E, we used monthly root-zone SM,
359 precipitation, evapotranspiration from the Modern-Era Retrospective analysis for Research and
360 Applications, version 2 (MERRA-2)[41] dataset (1980-2018), and the European Centre for Medium-
361 Range Weather Forecasts (ERA5, 1979-2018). In ERA5, we used 0-100cm SM to approximate
362 root-zone SM. As the two reanalysis datasets are constrained by *in situ* and satellite remote sensing
363 observations, they largely reflect the relationship between SM and P-E.
364
365 To further understand how SM impacts P-E, we used vertically integrated moisture convergence
366 (MC) and decomposed MC into mean flow convergence and transient eddy convergence, using
367 monthly specific humidity and eastward and northward wind at all pressure levels (0-1000 hPa),
368 and surface pressure from ERA5 and MERRA2 (see "Moisture Convergence Decomposition"
369 below). We also used monthly pressure velocity at 700 hPa, which provides a good representation
370 of the middle tropospheric circulation, from ERA5 and MERRA2 to assess the SM effect on
371 atmospheric vertical motion.
372
373 **Definition of drylands.** Drylands are generally defined as regions with an aridity index (the ratio
374 of precipitation to potential evapotranspiration, $P/E_0$) less than 0.65[42]. There are numerous ways
375 to estimate $E_0$ under certain climatic conditions[43], which may result in varying definitions of
376 drylands. A good $E_0$ estimation can well predict mean annual evapotranspiration (E) through the
377 Budyko functions[44]. A widely used analytical Budyko function[45] is

$$\frac{E}{P} = \frac{1}{\left[\left(\frac{E_0}{P}\right)^{-n} + 1\right]^{\frac{1}{n}}} \quad (2)$$

The parameter $n$ represents the influence of land characteristics on E. Comparing existing Budyko functions, the Pike's equation ($n$=2.0) is closest to the original Budyko curve[44]. Using the Pike's equation to describe the relationship between E/P and $E_0$/P, we obtained a E/P ratio of 0.84 when P/$E_0$ is set as the threshold of 0.65. In other words, drylands are identified as regions where E/P is greater than 0.84. Noting that climate models do not produce $E_0$, but do simulate E and P, we therefore defined drylands as regions where multi-model mean E/P is larger than 0.84 in the historical period (1971-2000) for CMIP5 and GLACE-CMIP5 (REF) models (Fig. S2a,c).

**The SM-(P-E) feedback.** Because SM and P-E are strongly coupled, it is difficult to isolate the SM feedback on P-E from the direct P-E impact on SM. A feedback has been quantified based on the temporally lagged correlation in many previous studies[46,47]. The difficulty in determining the SM-(P-E) feedback is mainly because of the persistent impact of P-E (especially P) on SM, as the slow processes of soil water percolation, evaporation, and transpiration lead to relatively long SM memory (weeks to months) of precipitation events[48]. The lagged correlation between SM and subsequent P-E therefore may reflect precipitation autocorrelation rather than the SM-(P-E) feedback[47]. Additionally, the seasonal cycles and long-term trends of P-E and SM also contribute to the lagged correlation[47], although they are largely driven by external factors such as regional climatology and global warming.

To address these issues, we established a multiple linear regression model between P-E and one-month lagged SM to assess the SM-(P-E) feedback.

$$(P-E)_d(t+1) = n_0 + n_1 \cdot SM_d(t) + n_2 \cdot (P-E)_d(t) \quad (3)$$

The subscript $d$ indicates that the multi-year mean seasonal cycle and the linear trend of the variable have been removed, and the indicator $t$ represents monthly steps. The lagged term $(P-E)_d(t)$ on the right side of equation (3) aims to remove the effect of P-E autocorrelation. Therefore, the regression coefficient $n_1$ ($\frac{\partial (P-E)_d(t+1)}{\partial SM_d(t)}$) represents the SM feedback on P-E. Although the SM-(P-E) feedback may be non-linear and time-dependent, the regression coefficient obtained from the linear model reflects the long-term mean effect of SM on P-E.

We used partial least square regression (PLSR)[49] to obtain the regression coefficient $n_1$ in equation (3). PLSR combines features of principal component analysis and multiple linear regression (MLR). It projects the predictor variables onto orthogonal principal components to overcome the issue of multicollinearity among predictor variables (i.e., the predictor variables are highly linearly related). PLSR then regresses the dependent variable against principal components to obtain regression slopes. We find that $(P-E)_d(t)$ and $SM_d(t)$ are weakly correlated in most grid cells. In these cases, PLSR obtains the same regression results as MLR. In case of a strong correlation between $(P-E)_d(t)$ and $SM_d(t)$ at some grid cells, we use PLSR instead of MLR to overcome the multicollinearity problem. To facilitate comparison of the SM-(P-E) feedback across different regions and in different datasets/models, we used PLSR standardized coefficients (or dimensionless sensitivity coefficients) corresponding to standardized $(P-E)_d$ and $SM_d$ of zero mean and unit variance (z-score) to measure the SM-(P-E) feedback.

As the SM-(P-E) feedback may be impacted by natural variability, we used a bootstrap test to determine the significance of the sensitivity coefficients. We performed bootstrap analyses with

500 realizations for the two reanalysis datasets (480 months for ERA5 and 468 months for MERRA-2) and 2000 realizations for fully coupled simulations of the four GLACE-CMIP5 models (1560 months, 1971-2100). The time series are randomly resampled to obtain the 95% confidence intervals of the sensitivity coefficients. We used the adjusted bootstrap percentile interval as different types of confidence intervals generate very similar results. According to the bootstrap confidence intervals, the sensitivity coefficients are deemed to be statistically significant if the 95% confidence intervals do not contain zero.

We also used similar multiple linear regression models and bootstrap tests to assess the SM feedbacks on evapotranspiration and precipitation. To demonstrate that the SM-atmosphere feedbacks are consistent between current and future climates, we use data from the fully coupled GLACE-CMIP5 simulations to compare the SM-atmosphere feedbacks: 1) between recent (1979-2018) and future (2061-2100) periods, and 2) by removing and retaining the long-term trends in the variables during the 1971-2100 period. Both comparisons show consistent strong positive SM→E, weak SM→P, and negative SM→(P-E) (Fig. 3a-c and Fig. S10). In particular, the spatial correlation coefficient for SM→(P-E) is 0.92 in comparison 1) and 0.97 in comparison 2), indicating that the negative SM-(P-E) feedback is robust to the presence of long-term climate change.

**Moisture Convergence Decomposition.** Atmospheric MC is calculated as the negative divergence of vertically integrated moisture flux over the pressure ($p$) from the top of the atmosphere ($p = 0$) to the surface ($p = p_s$).

$$MC = -\frac{1}{\rho_w g}\nabla \cdot \int_0^{p_s} (\boldsymbol{u}q)dp \quad (4)$$

$\rho_w$ is the density of water, $g$ is the acceleration due to gravity, $\nabla$ is the horizontal divergence operator, $\boldsymbol{u}$ is the horizontal vector wind, and $q$ is specific humidity.

At the monthly scale, MC can be decomposed into mean flow convergence (MFC) determined by atmospheric mean wind and moisture fields and transient eddy convergence (TEC) by highly variable (hourly to daily) wind and moisture fields within storm systems[29].

$$MC = -\frac{1}{\rho_w g}\nabla \cdot \int_0^{p_s} (\overline{\boldsymbol{u}}\,\overline{q} + \overline{\boldsymbol{u}'q'})dp \tag{5}$$

$$MFC = -\frac{1}{\rho_w g}\nabla \cdot \int_0^{p_s} (\overline{\boldsymbol{u}}\,\overline{q})dp \tag{6}$$

$$TEC = -\frac{1}{\rho_w g}\nabla \cdot \int_0^{p_s} (\overline{\boldsymbol{u}'q'})dp \tag{7}$$

Overbars indicate monthly mean values, and primes represent departures from the monthly mean values.

Using climatological monthly values of $\overline{\boldsymbol{u}}$ and $\overline{q}$ as reference, monthly MFC anomalies ($\delta MFC$) can be further decomposed into three components[30]: 1) a thermodynamic component ($\delta TH$) induced by specific humidity anomalies, 2) a mean circulation dynamic component ($\delta MCD$) induced by horizontal wind anomalies, and 3) a covariation component ($\delta COV$) induced by the product of specific humidity anomalies and horizontal wind anomalies.

$$\delta MFC = -\frac{1}{\rho_w g}\nabla \cdot \int_0^{p_s} (\overline{\boldsymbol{u}}_0\delta\overline{q} + \overline{q}_0\delta\overline{\boldsymbol{u}} + \delta\overline{\boldsymbol{u}}\delta\overline{q})dp \tag{8}$$

$$\delta TH = -\frac{1}{\rho_w g}\nabla \cdot \int_0^{p_s} (\overline{\boldsymbol{u}}_0\delta\overline{q})dp \tag{9}$$

$$\delta MCD = -\frac{1}{\rho_w g}\nabla \cdot \int_0^{p_s} (\overline{q}_0\delta\overline{\boldsymbol{u}})dp \tag{10}$$

$$\delta COV = -\frac{1}{\rho_w g}\nabla \cdot \int_0^{p_s} (\delta\overline{\boldsymbol{u}}\delta\bar{q})dp \quad (11)$$

The subscript 0 represents climatological monthly values and $\delta$ represents departure from the monthly climatology.

**Attribution analysis.** We used a variance decomposition method[50,51] to assess contributions of each MC component to monthly variations in MC. We removed the long-term trends and seasonal cycles to focus on the sub-seasonal and inter-annual variations in MC.

$$MC_d = MFC_d + TEC_d \quad (12)$$

As in equation (3), the subscript $d$ indicates the variable is linearly detrended and deseasonalized. The variance of $MC_d$ ($var(MC_d)$) can be decomposed into its covariance with the two components on the right side of equation (12).

$$var(MC_d) = cov(MC_d, MFC_d) + cov(MC_d, TEC_d) \quad (13)$$

The contributions of $MFC_d$ ($R(MC, MFC)$) and $TEC_d$ ($R(MC, TEC)$) to $MC_d$ variations in MERRA2 (1980-2018) and ERA5 (1979-2018) are therefore calculated as

$$R(MC, MFC) = \frac{cov(MC_d, MFC_d)}{var(MC_d)} \quad (14)$$

$$R(MC, TEC) = \frac{cov(MC_d, TEC_d)}{var(MC_d)} \quad (15)$$

Similarly, we assessed contributions of the three components of $MFC_d$ to $MC_d$ variations. The separated contributions of $MFC_d$, $TEC_d$ and the three components of $MFC_d$ to $MC_d$ variations are shown in Fig. S8.

**Data availability.** The GLACE-CMIP5 simulations are available from S.I.S. (sonia.seneviratne@ethz.ch) and the climate modelling groups upon reasonable request. All other data used in this study are available online. The CMIP5 model simulations are from https://esgf-node.llnl.gov/search/cmip5/. The ERA5 reanalysis data are from https://www.ecmwf.int/en/forecasts/datasets/archive-datasets/reanalysis-datasets/era5. The MERRA-2 reanalysis data are from https://gmao.gsfc.nasa.gov/reanalysis/MERRA-2/data_access/.

**Code availability.** The code used for modelling and reanalysis data analyses is available from https://github.com/shazhou09/dryland_water_availability.

Correspondence and requests for materials should be addressed to S.Z..

**Acknowledgements**

We acknowledge the World Climate Research Programme's Working Group on Coupled Modelling, which is responsible for CMIP, and we thank the climate modeling groups (listed in Table S1 of this paper) for producing and making available their model output. For CMIP the U.S. Department of Energy's Program for Climate Model Diagnosis and Intercomparison provides coordinating support and led development of software infrastructure in partnership with the Global Organization for Earth System Science Portals. S.Z. acknowledges support from the Lamont-Doherty Postdoctoral Fellowship and the Earth Institute Postdoctoral Research Program. P.G. acknowledges support from NASA ROSES Terrestrial hydrology (NNH17ZDA00IN-THP) and NOAA MAPP NA17OAR4310127. A.P.W. and B.I.C. acknowledge support from the NASA

Modeling, Analysis, and Prediction (MAP) program (NASA 80NSSC17K0265). T.F.K. acknowledges support from the RUBISCO SFA, which is sponsored by the Regional and Global Model Analysis (RGMA) Program in the Climate and Environmental Sciences Division (CESD) of the Office of Biological and Environmental Research (BER) in the U.S. Department of Energy Office of Science. We also acknowledge Richard Seager and Jason Smerdon from Lamont-Doherty Earth Observatory of Columbia University for insightful discussion and techincal assistance with and interpretation of the moisture convergence decomposition (R.S.).

**Author contributions**

S.Z. conceived and designed the study. S.Z. processed model simulations and reanalysis data. S.Z., A.P.W., B.R.L., A.M.B., Y.Z., T.F.K., B.I.C., S.H., S.I.S. and P.G. contributed to data analysis and interpretation. S.Z. drafted the manuscript. All authors edited the manuscript.

**Competing financial interests**

The authors declare no competing financial interests.

**References:**

1. Oki, T. & Kanae, S. Global Hydrological Cycles and World Water Resources. *Science* **313**, 1068–1072 (2006).
2. Rockström, J. *et al.* Future water availability for global food production: The potential of green water for increasing resilience to global change. *Water Resources Research* (2018) doi:10.1029/2007WR006767@10.1002/(ISSN)1944-7973.LANDUSE1.

3. Anderegg, W. R. L. *et al.* Tree mortality predicted from drought-induced vascular damage. *Nature Geosci* **8**, 367–371 (2015).
4. Ruppert, J. C. *et al.* Quantifying drylands' drought resistance and recovery: the importance of drought intensity, dominant life history and grazing regime. *Glob Change Biol* **21**, 1258–1270 (2015).
5. Huntington, T. G. Evidence for intensification of the global water cycle: Review and synthesis. *Journal of Hydrology* **319**, 83–95 (2006).
6. Held, I. M. & Soden, B. J. Robust Responses of the Hydrological Cycle to Global Warming. *J. Climate* **19**, 5686–5699 (2006).
7. Lorenz, D. J. & DeWeaver, E. T. The Response of the Extratropical Hydrological Cycle to Global Warming. *J. Climate* **20**, 3470–3484 (2007).
8. Greve, P. & Seneviratne, S. I. Assessment of future changes in water availability and aridity. *Geophysical Research Letters* **42**, 5493–5499 (2015).
9. Byrne, M. P. & O'Gorman, P. A. The Response of Precipitation Minus Evapotranspiration to Climate Warming: Why the "Wet-Get-Wetter, Dry-Get-Drier" Scaling Does Not Hold over Land. *J. Climate* **28**, 8078–8092 (2015).
10. Chou, C., Neelin, J. D., Chen, C.-A. & Tu, J.-Y. Evaluating the "Rich-Get-Richer" Mechanism in Tropical Precipitation Change under Global Warming. *J. Climate* **22**, 1982–2005 (2009).
11. Vecchi, G. A. *et al.* Weakening of tropical Pacific atmospheric circulation due to anthropogenic forcing. *Nature* **441**, 73–76 (2006).
12. Chadwick, R., Boutle, I. & Martin, G. Spatial Patterns of Precipitation Change in CMIP5: Why the Rich Do Not Get Richer in the Tropics. *J. Climate* **26**, 3803–3822 (2012).

554 13. Guillod, B. P., Orlowsky, B., Miralles, D. G., Teuling, A. J. & Seneviratne, S. I.
555 Reconciling spatial and temporal soil moisture effects on afternoon rainfall. *Nature*
556 *Communications* **6**, 6443 (2015).
557 14. Seneviratne, S. I. *et al.* Investigating soil moisture–climate interactions in a changing
558 climate: A review. *Earth-Science Reviews* **99**, 125–161 (2010).
559 15. Taylor, C. M., Parker, D. J. & Harris, P. P. An observational case study of mesoscale
560 atmospheric circulations induced by soil moisture. *Geophysical Research Letters* **34**, (2007).
561 16. Ookouchi, Y., Segal, M., Kessler, R. C. & Pielke, R. A. Evaluation of Soil Moisture
562 Effects on the Generation and Modification of Mesoscale Circulations. *Mon. Wea. Rev.* **112**,
563 2281–2292 (1984).
564 17. Segal, M. & Arritt, R. w. Nonclassical Mesoscale Circulations Caused by Surface
565 Sensible Heat-Flux Gradients. *Bull. Amer. Meteor. Soc.* **73**, 1593–1604 (1992).
566 18. Taylor, C. M., de Jeu, R. A. M., Guichard, F., Harris, P. P. & Dorigo, W. A. Afternoon
567 rain more likely over drier soils. *Nature* **489**, 423–426 (2012).
568 19. Hsu, H., Lo, M.-H., Guillod, B. P., Miralles, D. G. & Kumar, S. Relation between
569 precipitation location and antecedent/subsequent soil moisture spatial patterns: Precipitation-
570 Soil Moisture Coupling. *J. Geophys. Res. Atmos.* **122**, 6319–6328 (2017).
571 20. Froidevaux, P., Schlemmer, L., Schmidli, J., Langhans, W. & Schär, C. Influence of the
572 Background Wind on the Local Soil Moisture–Precipitation Feedback. *J. Atmos. Sci.* **71**, 782–
573 799 (2013).
574 21. Seneviratne, S. I. *et al.* Impact of soil moisture-climate feedbacks on CMIP5 projections:
575 First results from the GLACE-CMIP5 experiment. *Geophysical Research Letters* **40**, 5212–
576 5217 (2013).

22. Byrne, M. P. & O'Gorman, P. A. Land–Ocean Warming Contrast over a Wide Range of Climates: Convective Quasi-Equilibrium Theory and Idealized Simulations. *J. Climate* **26**, 4000–4016 (2012).

23. Joshi, M. M., Gregory, J. M., Webb, M. J., Sexton, D. M. H. & Johns, T. C. Mechanisms for the land/sea warming contrast exhibited by simulations of climate change. *Clim Dyn* **30**, 455–465 (2008).

24. Fasullo, J. T. Robust Land–Ocean Contrasts in Energy and Water Cycle Feedbacks. *J. Climate* **23**, 4677–4693 (2010).

25. Tokinaga, H., Xie, S.-P., Deser, C., Kosaka, Y. & Okumura, Y. M. Slowdown of the Walker circulation driven by tropical Indo-Pacific warming. *Nature* **491**, 439–443 (2012).

26. Lu, J., Vecchi, G. A. & Reichler, T. Expansion of the Hadley cell under global warming. *Geophysical Research Letters* **34**, (2007).

27. Karnauskas, K. B. & Ummenhofer, C. C. On the dynamics of the Hadley circulation and subtropical drying. *Clim Dyn* **42**, 2259–2269 (2014).

28. Lau, W. K. M. & Kim, K.-M. Robust Hadley Circulation changes and increasing global dryness due to $CO_2$ warming from CMIP5 model projections. *Proc Natl Acad Sci USA* **112**, 3630–3635 (2015).

29. Seager, R. *et al.* Model Projections of an Imminent Transition to a More Arid Climate in Southwestern North America. *Science* **316**, 1181–1184 (2007).

30. Seager, R., Naik, N. & Vecchi, G. A. Thermodynamic and Dynamic Mechanisms for Large-Scale Changes in the Hydrological Cycle in Response to Global Warming. *J. Climate* **23**, 4651–4668 (2010).

31. O'Gorman, P. A. & Schneider, T. Stochastic Models for the Kinematics of Moisture Transport and Condensation in Homogeneous Turbulent Flows. *J. Atmos. Sci.* **63**, 2992–3005 (2006).

32. He, J. & Soden, B. J. A re-examination of the projected subtropical precipitation decline. *Nature Climate Change* **7**, 53–57 (2017).

33. Chadwick, R., Ackerley, D., Ogura, T. & Dommenget, D. Separating the Influences of Land Warming, the Direct CO2 Effect, the Plant Physiological Effect, and SST Warming on Regional Precipitation Changes. *Journal of Geophysical Research: Atmospheres* **124**, 624–640 (2019).

34. Findell, K. L. *et al.* Rising Temperatures Increase Importance of Oceanic Evaporation as a Source for Continental Precipitation. *Journal of Climate* **32**, 7713–7726 (2019).

35. Krakauer, N. Y., Cook, B. I. & Puma, M. J. Contribution of soil moisture feedback to hydroclimatic variability. *Hydrol. Earth Syst. Sci.* 16 (2010).

36. Roudier, P. *et al.* Projections of future floods and hydrological droughts in Europe under a +2°C global warming. *Climatic Change* **135**, 341–355 (2016).

37. Zhou, S., Zhang, Y., Williams, A. P. & Gentine, P. Projected increases in intensity, frequency, and terrestrial carbon costs of compound drought and aridity events. *Science Advances* **5**, eaau5740 (2019).

38. Lorenz, R. *et al.* Influence of land-atmosphere feedbacks on temperature and precipitation extremes in the GLACE-CMIP5 ensemble. *Journal of Geophysical Research: Atmospheres* **121**, 607–623 (2016).

39. Berg, A. *et al.* Land–atmosphere feedbacks amplify aridity increase over land under global warming. *Nature Climate Change* **6**, 869–874 (2016).

40. Zhou, S. *et al.* Land–atmosphere feedbacks exacerbate concurrent soil drought and atmospheric aridity. *PNAS* 201904955 (2019) doi:10.1073/pnas.1904955116.

41. Gelaro, R. *et al.* The Modern-Era Retrospective Analysis for Research and Applications, Version 2 (MERRA-2). *J. Climate* **30**, 5419–5454 (2017).

42. Huang, J., Yu, H., Guan, X., Wang, G. & Guo, R. Accelerated dryland expansion under climate change. *Nature Climate Change* **6**, 166–171 (2016).

43. Milly, P. C. D. & Dunne, K. A. Potential evapotranspiration and continental drying. *Nature Climate Change* **6**, 946–949 (2016).

44. Zhou, S., Yu, B., Huang, Y. & Wang, G. The complementary relationship and generation of the Budyko functions. *Geophysical Research Letters* **42**, 1781–1790 (2015).

45. Choudhury, BhaskarJ. Evaluation of an empirical equation for annual evaporation using field observations and results from a biophysical model. *Journal of Hydrology* **216**, 99–110 (1999).

46. Wei, J., Dickinson, R. E. & Chen, H. A Negative Soil Moisture–Precipitation Relationship and Its Causes. *J. Hydrometeor.* **9**, 1364–1376 (2008).

47. Zhang, J., Wang, W.-C. & Wei, J. Assessing land-atmosphere coupling using soil moisture from the Global Land Data Assimilation System and observational precipitation. *J. Geophys. Res.* **113**, D17119 (2008).

48. Seneviratne, S. I. *et al.* Soil Moisture Memory in AGCM Simulations: Analysis of Global Land–Atmosphere Coupling Experiment (GLACE) Data. *J. Hydrometeor.* **7**, 1090–1112 (2006).

49. Geladi, P. & Kowalski, B. R. Partial least-squares regression: a tutorial. *Analytica Chimica Acta* **185**, 1–17 (1986).

50. Zhou, S. *et al.* Sources of Uncertainty in Modeled Land Carbon Storage within and across Three MIPs: Diagnosis with Three New Techniques. *J. Climate* **31**, 2833–2851 (2018).

51. Zhou, S. *et al.* Response of Water Use Efficiency to Global Environmental Change Based on Output From Terrestrial Biosphere Models: Drivers of WUE Variability. *Global Biogeochemical Cycles* **31**, 1639–1655 (2017).